ICAS-90-1.5.1

NEAR-OPTIMAL GUIDANCE TRAJECTORIES FOR COPLANAR, AEROASSISTED ORBITAL TRANSFER[1,2]

A. Miele[3] and T. Wang[4]

Rice University, Houston, Texas

Abstract. This paper is concerned with the optimization and guidance of trajectories for coplanar, aeroassisted orbital transfer (AOT) from high Earth orbit (HEO) to low Earth orbit (LEO). In particular, HEO can be a geosynchronous Earth orbit (GEO).

First, optimal trajectories are computed by minimizing the total velocity impulse (hence, the propellant consumption) required for AOT transfer. It is shown that the optimal trajectory includes two branches: a relatively short descending flight branch (branch 1) and a long ascending flight branch (branch 2).

Next, attention is focused on guidance trajectories. For the atmospheric pass, a feedback control scheme is employed and the lift coefficient is adjusted according to a two-stage gamma guidance law. For branch 1, the gamma guidance is a linear path inclination guidance; for branch 2, the gamma guidance is a constant path inclination guidance. The selection of the guidance parameters (entry path inclination, target altitude, switch velocity, and target path inclination) is discussed.

Further improvements are possible via a modified gamma guidance, which differs from the gamma guidance in two aspects: lower target altitude; and use of a predictor-corrector algorithm to determine the switch velocity and the target path inclination. Computer simulations show that, vis-a-vis the gamma guidance, the modified gamma guidance is more stable with respect to dispersion effects arising from navigation errors, variations of the atmospheric density, and uncertainties in the aerodynamic coefficients.

Key Words. Optimization, guidance, gamma guidance, modified gamma guidance, parameter dispersion effects, flight mechanics, astrodynamics, aeroassisted orbital transfer, sequential gradient-restoration algorithm.

Nomenclature

C_D = drag coefficient;

C_{D0} = zero-lift drag coefficient;

---

[1]Paper presented at the 17th Congress of the International Council of the Aeronautical Sciences, Stockholm, Sweden, September 10-14, 1990 (Paper No. ICAS-90-151).

[2]This research was supported by Jet Propulsion Laboratory, by NASA Marshall Space Flight Center, and by Texas Advanced Technology Program.

[3]Foyt Family Professor of Aerospace Sciences and Mathematical Sciences, Aero-Astronautics Group. Fellow AIAA.

[4]Senior Research Scientist, Aero-Astronautics Group. Member AIAA.

C_L = lift coefficient;

D = drag, N;

g = local acceleration of gravity, m/sec^2;

h = altitude, m;

H = $r_a - r_e$ = thickness of the atmosphere, m;

HR = heating rate, W/m^2;

K = induced drag factor;

K = gain coefficient;

L = lift, N;

m = mass, kg;

r = radial distance from the center of the Earth, m;

r_e = radius of the Earth, m;

r_a = radius of the outer edge of the atmosphere, m;

S = reference surface area, m^2;

t = T/τ = dimensionless time;

T = running time, sec;

V = velocity, m/sec;

V_a = $\sqrt{(\mu/r_a)}$ = circular velocity at $r = r_a$, m/sec;

γ = path inclination, rad;

μ = Earth's gravitational constant, m^3/sec^2;

ρ = air density, kg/m^3;

τ = final time, sec;

ΔV = characteristic velocity, m/sec.

Subscripts

0 = entry into the atmosphere;

1 = exit from the atmosphere;

00 = exit from the initial orbit;

11 = entry into the final orbit.

Superscripts

. = derivative with respect to dimensionless time;

~ = condition following the application of a velocity impulse or nominal condition.

1. Introduction

Saving propellant weight and increasing the payload are among the most important problems of space transportation. Orbital transfer from high Earth orbit (HEO) to low Earth orbit (LEO) can be made more economic if the aeroassisted orbital transfer (AOT) mode is employed. In the AOT mode, use is made of the aerodynamic forces in order to achieve the proper amount of velocity depletion during the atmospheric pass. Here, the intent is to achieve a specified apogee following the atmospheric exit, while minimizing the overall propellant consumption and keeping the peak heating rate within reasonable bounds during the atmospheric pass.

Aeroassisted orbital transfer is not only important for HEO-to-LEO transfer maneuvers, but may prove to be indispensable for future planetary flights. In particular, this statement refers to lunar return vehicles, Mars exploration vehicles, and Mars return vehicles.

Over the past several years, considerable research has been done on two aspects of coplanar, aeroassisted orbital transfer: trajectory optimization (Refs. 1-5) and trajectory guidance (Refs. 6-10). In particular, in Ref. 10, a two-stage guidance scheme, consisting of the combination of target altitude guidance and target path inclination guidance, was developed for the atmospheric pass of an

AOT spacecraft, akin to the target altitude guidance already developed for the abort landing of an aircraft in a windshear (Ref. 11).

This paper continues the work of Ref. 10 and develops a two-stage gamma guidance for the atmospheric pass of an AOT spacecraft, akin to the gamma guidance already developed for the abort landing of an aircraft in a windshear (Ref. 12). Indeed, there are similarities between these two situations: (i) both trajectories are characterized by descending flight, followed by near-horizontal flight, followed by ascending flight; (ii) both trajectories are characterized by energy dissipation; (iii) both trajectories are dangerous unless proper guidance and control are applied. However, there are also differences between these two situations: (i) the performance index of the AOT spacecraft is the characteristic velocity, while the performance index of the abort landing aircraft is the altitude drop; (ii) the energy dissipation of the AOT spacecraft is due to the aerodynamic forces, while the energy dissipation of the abort landing aircraft is due to the combination of shear and downdraft; (iii) reaching a specified apogee after the atmospheric pass is essential for the AOT spacecraft, while reaching a specified altitude after the windshear encounter is not essential for the abort landing aircraft. The similarities suggest that the gamma guidance scheme developed for abort landing in a windshear can be adapted in concept to the atmospheric pass of an AOT spacecraft. The differences suggest that major modifications are necessary.

With the above ideas in mind, this paper is organized as follows. First, we describe the system and study optimal trajectories, namely, trajectories minimizing the propellant consumption required for orbital transfer. Then, we develop gamma guidance trajectories so as to approximate the optimal trajectories. Next, we develop modified gamma guidance trajectories in order to improve the stability with respect to dispersion effects arising from navigation errors, variations of the atmospheric density,and uncertainties in the aerodynamic coefficients.Finally,we give the conclusions.

2. System Description

In this section, we consider coplanar, aeroassisted orbital transfer from high Earth orbit to low Earth orbit. We employ the following assumptions: (i) the initial and final orbits are circular; (ii) three impulses are employed, one at the exit from the initial orbit, one at the exit from the atmosphere, and one at the entry into the final orbit; and (iii) the gravitational field is central and is governed by the inverse square law. The four key points of the maneuver are these: point 00, exit from the initial orbit; point 0, entry into the atmosphere; point 1, exit from the atmosphere; and point 11, entry into the final orbit; see Fig. 1.

The maneuver starts in high Earth orbit with a tangential propulsive burn,

having characteristic velocity ΔV_{00}, at point 00; here, the spacecraft enters into an elliptical transfer orbit, connecting the points 00 and 0; this elliptical transfer orbit is such that its apogee occurs at r_{00}. At point 0, the spacecraft enters into the atmosphere; after traversing the upper layers of the atmosphere, it exits from the atmosphere at point 1; during the atmospheric pass, the velocity of the spacecraft is depleted, due to the aerodynamic drag. At point 1, the maneuver continues with a tangential propulsive burn, having characteristic velocity ΔV_1; then, the spacecraft enters into an elliptical transfer orbit connecting the points 1 and 11; this elliptical transfer orbit is such that its apogee occurs at r_{11}. The maneuver ends with a tangential propulsive burn, having characteristic velocity ΔV_{11}, at point 11; here, the spacecraft enters into low Earth orbit,in that the magnitude of ΔV_{11} is such that the desired circularization into LEO is achieved.

2.1. Atmospheric Pass. For the atmospheric portion of the trajectory of the AOT vehicle, we employ the following hypotheses: (i) the atmospheric pass is made with engine shut-off; hence, in this portion of the flight, the AOT vehicle behaves as a particle of constant mass; (ii) Coriolis acceleration terms and transport acceleration terms are neglected; (iii) the spacecraft is controlled via the lift coefficient; (iv) the aerodynamic forces are evaluated using the inertial velocity, rather than the relative velocity; (v) under extreme hypersonic conditions, the dependence of the aerodynamic coefficients on the Mach number and the Reynolds number is disregarded.

2.2. Differential System. With the above assumptions, and upon normalizing the flight time to unity, the equations of motion are given by

$$\dot{h} = \tau[V\sin\gamma], \tag{1a}$$

$$\dot{V} = \tau[-D/m - g\sin\gamma], \tag{1b}$$

$$\dot{\gamma} = \tau[L/mV + (V/r - g/V)\cos\gamma], \tag{1c}$$

with $0 \leq t \leq 1$. In the above equations,

$$r = r_e + h, \quad g = \mu/r^2 = \mu/(r_e + h)^2, \tag{2}$$

where μ denotes the Earth's gravitational constant. In addition, the aerodynamic forces are given by

$$D = (1/2)C_D\rho SV^2, \quad L = (1/2)C_L\rho SV^2, \tag{3a}$$

with $\rho = \rho(h)$. In particular, if a parabolic polar is postulated, the relation between the drag coefficient and the lift coefficient is given by

$$C_D = C_{D0} + KC_L^2. \tag{3b}$$

2.3. Control Constraint. To obtain realistic solutions, the presence of upper and lower bounds on the lift coefficient is necessary. Therefore, the two-sided inequality constraint

$$C_{La} \leq C_L \leq C_{Lb} \tag{4}$$

must be satisfied everywhere along the

interval of integration.

2.4. Boundary Conditions. At the entry into the atmosphere (t = 0) and at the exit from the atmosphere (t = 1), certain static and dynamic boundary conditions must be satisfied. Specifically, at atmospheric entry, we have

$$h_0 = H, \tag{5a}$$

$$r_{00}^2(2V_a^2 - V_0^2) - 2r_{00}r_aV_a^2 + r_a^2V_0^2\cos^2\gamma_0 = 0. \tag{5b}$$

In addition, at atmospheric exit, we have

$$h_1 = H, \tag{6a}$$

$$r_{11}^2(2V_a^2 - \tilde{V}_1^2) - 2r_{11}r_aV_a^2 + r_a^2\tilde{V}_1^2\cos^2\gamma_1 = 0. \tag{6b}$$

Because the velocity impulse ΔV_1 is applied at atmospheric exit, the following relation holds:

$$\Delta V_1 = \tilde{V}_1 - V_1, \tag{7a}$$

where V_1 and $\tilde{V}_1$ denote the values of the exit velocity before and after the application of the propellant burn. In the light of the exit condition (6b), the value of the exit velocity after the application of the propellant burn can be written as

$$\tilde{V}_1 = V_a\sqrt{[2(r_{11}^2 - r_{11}r_a)/(r_{11}^2 - r_a^2\cos^2\gamma_1)]}. \tag{7b}$$

2.5. Experimental Data. The following data are used in the numerical experiments for optimal trajectories and guidance trajectories.

Spacecraft. For the spacecraft, it is assumed that the mass per unit reference surface area is $m/S = 300$ kg/m^2; the zero-lift drag coefficient is $C_{D0} = 0.1$; the induced drag factor is $K = 1.11$; the lift coefficient for maximum lift-to-drag ratio is $C_{LE} = 0.3$; the maximum lift-to-drag ratio is $E_{max} = 1.5$; the bounds on the lift coefficient are $C_{La} = -0.9$ and $C_{Lb} = +0.9$.

Physical Constants. The major physical constants used in the computations are as follows: the radius of the Earth is $r_e = 6378$ km; the radius of the outer edge of the atmosphere is $r_a = 6498$ km; the thickness of the atmosphere is $H = 120$ km; and the Earth's gravitational constant is $\mu = 0.3986E{+}06$ km^3/sec^2.

Transfer Maneuvers. Three transfer maneuvers are considered, involving different values of the HEO radius, but the same value of the LEO radius. To describe these maneuvers, let α and β denote the dimensionless ratios

$$\alpha = r_{00}/r_a, \quad \beta = r_{11}/r_a. \tag{8}$$

Case 1. The HEO1 radius is $r_{00} = 12996$ km, $\alpha = 2$. The LEO radius is $r_{11} = 6558$ km, $\beta = 1.00923$.

Case 2. The HEO2 radius is $r_{00} = 25992$ km, $\alpha = 4$. The LEO radius is $r_{11} = 6558$ km, $\beta = 1.00923$.

Case 3. The HEO3 radius is $r_{00} = 42164$ km, $\alpha = 6.48877$. The LEO radius is $r_{11} = 6558$ km, $\beta = 1.00923$. Note that HEO3 = GEO.

Atmospheric Model. The atmospheric model assumed is that of the US Standard Atmosphere, 1976 (Ref. 13).

Heating Rate. The heating rate HR is computed with the relation

$$HR = C\sqrt{(\rho/\rho_R)}\,(V/V_R)^{3.08}. \qquad (9)$$

Here, ρ_R = 0.39957E-02 kg/m^3 is a reference density (density at the reference altitude h_R = 40 km) and V_R = V_a = 7.832 km/sec is a reference velocity. The constant C represents the heating rate at $V = V_R$ and $h = h_R$; its value is assumed to be C = 348.7 W/cm^2.

3. Optimal Trajectories

3.1. Performance Index. Subject to the previous constraints, different AOT optimization problems can be formulated, depending on the performance index chosen. The resulting optimal control problems are either of the Bolza type or of the Chebyshev type. In this paper, only one performance index is considered, the minimum energy required for orbital transfer. A measure of this energy is the total characteristic velocity ΔV, the sum of the characteristic velocity ΔV_{00} associated with the propulsive burn from the initial orbit, the characteristic velocity ΔV_1 associated with the propulsive burn at the exit of the atmosphere, and the characteristic velocity ΔV_{11} associated with the propulsive burn into the final orbit. Clearly,

$$I = \Delta V = \Delta V_{00} + \Delta V_1 + \Delta V_{11}, \qquad (10a)$$

with

$$\Delta V_{00} = \sqrt{(r_a/r_{00})}\,V_a - (r_a/r_{00})V_0\cos\gamma_0, \qquad (10b)$$

$$\Delta V_1 = \tilde{V}_1 - V_1, \qquad (10c)$$

$$\Delta V_{11} = \sqrt{(r_a/r_{11})}\,V_a - (r_a/r_{11})\tilde{V}_1\cos\gamma_1. \qquad (10d)$$

In the last two equations, $\tilde{V}_1$ is supplied by Eq. (7b).

3.2. Numerical Results. Optimal trajectories were computed by minimizing the performance index (10), subject to the constraining relations. Three transfer maneuvers were considered: HEO1-to-LEO, HEO2-to-LEO, and HEO3-to-LEO; see Cases 1,2,3 of Section 2. The sequential gradient-restoration algorithm was employed in primal form (Refs. 14-16). This is a first-order algorithm which generates a sequence of feasible solutions, each characterized by a lower value of the performance index (10). The numerical results are shown in Table 1 and Fig. 2, which contains four parts: the altitude profile h(t), the velocity profile V(t), the path inclination profile $\gamma(t)$, and the lift coefficient profile $C_L(t)$. From Table 1 and Fig. 2, the following comments arise:

(i) The optimal trajectory includes two branches: a relatively short descending flight branch (branch 1) and a long ascending flight branch (branch 2). As the HEO radius increases, the minimum altitude of the optimal trajectory decreases, implying that a deeper penetration into the atmosphere is required to ensure the proper amount of velocity depletion.

(ii) Velocity depletion takes place along the entire atmospheric trajectory,but

is concentrated mostly in the terminal part of branch 1 and the beginning part of branch 2.

(iii) The path inclination increases rapidly from the entry value (a few degrees negative) to zero value in branch 1; and it increases slowly from zero value to the exit value (a fraction of a degree positive) in branch 2.

(iv) The lift coefficient profile is nearly independent of the HEO radius. In branch 1, the lift coefficient decreases rapidly from the upper bound value to nearly the lower bound value; in branch 2, the lift coefficient stays near the lower bound value.

3.3. Guidance Implications. Consider the altitude-path inclination domain and, with reference to Fig. 2, regard the altitude profile $h = h(t)$ and the path inclination profile $\gamma = \gamma(t)$ as parametric representation of the trajectory, the time t being the parameter. Upon elimination of the time, one obtains the path inclination-altitude relation $\gamma = \gamma(h)$. Then, this relation can be rewritten in the normalized form $\theta = \theta(\eta)$, where θ and η denote normalized variables defined as follows:

$$\theta = \gamma/|\gamma_0|, \quad \text{branch 1,} \tag{11a}$$

$$\theta = \gamma/|\gamma_0|, \quad \text{branch 2,} \tag{11b}$$

and

$$\eta = (h_0-h)/(h_0-h_{min}), \quad \text{branch 1,} \tag{12a}$$

$$\eta = (h-h_{min})/(h_0-h_{min}), \quad \text{branch 2.} \tag{12b}$$

The normalized path inclination-altitude relation $\theta = \theta(\eta)$ is plotted in Fig. 3, which contains two parts: the descending flight branch and the ascending flight branch. For branch 1, the normalized path inclination is nearly a linear function of the normalized altitude, and its slope is relatively steep; for branch 2, the normalized path inclination is also nearly a linear function of the normalized altitude, but its slope is relatively shallow. These observations are the basis of the gamma guidance law described in Section 4. This is a two-stage guidance law, designed as follows: for branch 1, the gamma guidance is a linear path inclination guidance; for branch 2, the gamma guidance is a constant path inclination guidance.

4. Gamma Guidance Trajectories

In the previous section, optimal trajectories (OT) for coplanar AOT flight were determined. They include three phases: the preatmospheric phase, characterized by the velocity impulse ΔV_{00} at HEO; the atmospheric phase, characterized by a relatively short descending flight branch (branch 1) and a long ascending flight branch (branch 2); and the postatmospheric phase, characterized by the velocity impulse ΔV_1 at atmospheric exit and the velocity impulse ΔV_{11} at LEO.

In this section, we develop gamma guidance trajectories (GGT) for coplanar AOT flight under two basic requirements: (a) the GGT should be close to the OT; and

(b) the GGT should be simple, easy to implement, and reliable. First, we discuss the space portion of the GGT; then,we discuss the atmospheric portion of the GGT.

4.1. Preatmospheric Phase. Initially, the spacecraft is in a high Earth orbit of radius r_{00}. To deorbit, the following velocity impulse is applied:

$$\Delta V_{00} = \sqrt{(r_a/r_{00})V_a - (r_a/r_{00})V_0 \cos\gamma_0}, \quad (13a)$$

with

$$V_0 = V_a\sqrt{[2(r_{00}^2 - r_{00}r_a)/ (r_{00}^2 - r_a^2\cos^2\gamma_0)]}. \quad (13b)$$

This enables the spacecraft to enter into an elliptical transfer orbit leading from HEO exit to atmospheric entry. In Eqs. (13), γ_0 is the entry path inclination and V_0 is the entry velocity. Because r_a, V_a are constant and r_{00} is given, Eqs. (13) imply that $V_0 = V_0(\gamma_0)$ and $\Delta V_{00} = \Delta V_{00}(\gamma_0)$. Hence, the selection of the entry angle γ_0 determines uniquely the entry velocity V_0 and the initial velocity impulse ΔV_{00}.

4.2. Postatmospheric Phase. The postatmospheric phase includes two velocity impulses: a velocity impulse ΔV_1 at atmospheric exit and a velocity impulse ΔV_{11} at LEO entry.

Atmospheric Exit. The velocity impulse at atmospheric exit is determined with the relation

$$\Delta V_1 = \tilde{V}_1 - V_1, \quad (14a)$$

where

$$\tilde{V}_1 = V_a\sqrt{[2(r_{11}^2 - r_{11}r_a)/ (r_{11}^2 - r_a^2\cos^2\gamma_1)]}. \quad (14b)$$

This velocity impulse is essential for the GGT in order to compensate for previous velocity errors. In Eqs. (14), γ_1 is the exit path inclination, V_1 is the exit velocity prior to the velocity impulse, and $\tilde{V}_1$ is the exit velocity after the velocity impulse. Note that r_a, V_a are constant, r_{11} is given, and V_1, γ_1 are measured in actual flight.

LEO Entry.After the velocity impulse (14) is applied, the spacecraft enters into an elliptical transfer orbit leading from atmospheric exit to LEO entry. This elliptical transfer orbit is such that its apogee occurs at r_{11}. At this point, the velocity impulse ΔV_{11} is applied so as to achieve circularization into LEO. Specifically, ΔV_{11} is determined with the relation

$$\Delta V_{11} = \sqrt{(r_a/r_{11})V_a} - V_{11}, \quad (15a)$$

in which V_{11} is the velocity at LEO entry prior to the velocity impulse. Note that r_a, V_a are constant, r_{11} is given, and V_{11} is measured in actual flight. However, in the computer simulations, the measurement of V_{11} is replaced by the relation

$$V_{11} = (r_a/r_{11})\tilde{V}_1\cos\gamma_1, \quad (15b)$$

which arises from angular momentum conservation applied to the exit-to-LEO transfer orbit. In Eq. (15b), $\tilde{V}_1$ is supplied by Eq. (14b).

4.3. Atmospheric Phase. The atmospheric phase includes the descending flight branch (branch 1) and the ascending flight branch (branch 2). For both branches, a gamma guidance scheme is implemented in feedback control form. The switch from branch 1 to branch 2 is regulated by the switch velocity V_S, to be selected appropriately.

Descending Flight Branch. For branch 1, the gamma guidance is a linear path inclination guidance, which is implemented in the following feedback control form:

$$C_L - \tilde{C}_L(h,V,\gamma) = -K_1(\gamma - \tilde{\gamma}), \tag{16a}$$

$$\tilde{\gamma} = \gamma_0(h - h_T)/(h_0 - h_T), \tag{16b}$$

$$C_{La} \leq C_L \leq C_{Lb}. \tag{16c}$$

Here, C_L is the instantaneous lift coefficient and $\tilde{C}_L$ is the nominal lift coefficient; C_{La} and C_{Lb} are the lower and upper bounds for the lift coefficient; γ is the instantaneous path inclination, $\tilde{\gamma}$ is the nominal path inclination, and γ_0 is the entry path inclination; h is the instantaneous altitude, h_0 is the entry altitude, and h_T is the target altitude; and K_1 is the gain coefficient for path inclination error.

The feedback form (16) of the gamma guidance is strongly stable at the target altitude; this is because $\tilde{\gamma} < 0$ if $h > h_T$, while $\tilde{\gamma} > 0$ if $h < h_T$. In addition, it avoids overshooting and undershooting of the target altitude, since $\tilde{\gamma}$ varies smoothly between the entry value $\tilde{\gamma} = \gamma_0$ and the target altitude value $\tilde{\gamma} = 0$.

Ascending Flight Branch. For branch 2, the gamma guidance is a constant path inclination guidance, which is implemented via the following feedback control form:

$$C_L - \tilde{C}_L(h,V,\gamma) = -K_2(\gamma - \tilde{\gamma}), \tag{17a}$$

$$\tilde{\gamma} = \gamma_T, \tag{17b}$$

$$C_{La} \leq C_L \leq C_{Lb}. \tag{17c}$$

Here, γ_T denotes the target path inclination and K_2 is the gain coefficient for path inclination error.

4.4. Comments on the Atmospheric Pass. The feedback control laws (16)-(17) require the specification of the nominal lift coefficient $\tilde{C}_L$, the gain coefficients K_1, K_2, plus four guidance parameters: the entry path inclination γ_0, the target altitude h_T, the switch velocity V_S, and the target path inclination γ_T. See the discussion below.

Nominal Lift Coefficient. The nominal lift coefficient $\tilde{C}_L$ is computed with Eq. (1c) under the assumption of near-equilibrium conditions. Upon setting $\dot{\gamma} \cong 0$, invoking Eqs. (2)-(3), and observing that $\rho = \rho(h)$, $r = r(h)$, and $g = g(h)$, we obtain the relation

$$(1/2)C_L\rho(h)SV^2+m[V^2/r(h)-g(h)]\cos\gamma=0, \tag{18a}$$

which admits the solution

$$\tilde{C}_L = 2m[g(h)-V^2/r(h)]\cos\gamma/\rho(h)SV^2, \tag{18b}$$

which has the form $\tilde{C}_L = \tilde{C}_L(h,V,\gamma)$.

Gain Coefficients. The gain coefficients for path inclination error are given by

$$K_1 = \rho_*/\rho, \quad K_2 = \rho_*/\rho, \tag{19}$$

where $\rho = \rho(h)$ is the air density at the altitude h and $\rho_* = \rho(h_*)$ is the air density at the reference altitude $h_* = H/3 = 40$ km. This particular form of the gain coefficients is justified by the need for a more energetic control response at higher altitudes and a gentler control response at lower altitudes.

Entry Path Inclination. The entry path inclination γ_0 should be in a proper range. If $|\gamma_0|$ is too small, the guidance trajectory is too flat, resulting in an early exit from the atmosphere; because not enough velocity is depleted in the atmospheric pass, this results in large values of the characteristic velocity. If $|\gamma_0|$ is too large, the guidance trajectory is too steep, resulting in deeper penetration of the atmosphere; therefore, the peak heating rate is too high.

Good results are obtained by choosing $|\gamma_0|$ of the GGT to be somewhat larger than $|\gamma_0|$ of the OT.

Target Altitude. The target altitude h_T should be in a proper range. If h_T is too high, the guidance trajectory is flat, resulting in an early exit from the atmosphere; because not enough velocity is depleted in the atmospheric pass, this results in large values of the characteristic velocity. If h_T is too low, the guidance trajectory is too steep, resulting in deeper penetration of the atmosphere; therefore, the peak heating rate is too high.

Good results are obtained by choosing h_T of the GGT to be somewhat lower than h_{min} of the OT. One option is to prescribe directly h_T; another option is to prescribe indirectly h_T, based on the selection of the target lift coefficient C_{LT}, corresponding to near-equilibrium level flight. The second option is preferable, because this procedure compensates automatically for variations of the atmospheric density with respect to the standard density; under this option, the target altitude is obtained from Eq. (18a) after inserting the relations

$$C_L = C_{LT}, \quad \gamma = 0, \tag{20a}$$

$$V = V_T = V_1 + 0.25(V_0 - V_1), \tag{20b}$$

where V_T denotes a reference velocity.

Switch Velocity. The switch velocity V_S should also be in a proper range. The best choice of V_S should be such that the exit velocity of the GGT is close to the exit velocity of the OT. If this is done, the velocity impulse at atmospheric exit ΔV_1 is small.

In practice, the switch velocity of the GGT is chosen to be a weighted average of the entry velocity of the OT and the exit velocity of the OT,

$$V_S = V_1 + A(V_0 - V_1), \tag{21}$$

where the dimensionless constant A is to be selected appropriately. Equation (21)

means that the switch velocity V_S is compatible with the target altitude h_T. Indeed, the higher the entry velocity V_0, the lower the minimum altitude h_{min} of the OT, hence the lower the target altitude h_T of the GT; to guarantee the same value of the exit velocity V_1, a higher switch velocity V_S is needed for the GT, which is the case with Eq.(21).

Target Path Inclination. The target path inclination γ_T should also be in a proper range. If γ_T is too small, the exit from the atmosphere might become physically impossible. If γ_T is too large, the characteristic velocity component ΔV_{11} might become too large.

In practice, the target path inclination of the GGT is chosen to be some fraction of the exit path inclination of the OT,

$$\gamma_T = B\gamma_1, \tag{22}$$

where the dimensionless constant B is to be selected appropriately.

4.5. Numerical Results. The four guidance parameters γ_0, h_T, V_S, γ_T were selected with the criteria of Section 4.4, and the corresponding guidance trajectories were computed. Table 2 shows the combinations of guidance parameters used for Case 1, Case 2, and Case 3. The resulting GGT is geometrically close to the corresponding OT, so as to retain the good features of the OT concerning the total characteristic velocity

$$\Delta V = \Delta V_{00} + \Delta V_1 + \Delta V_{11} \tag{23}$$

and the peak heating rate. The major conclusions are as follows:

(i) The functions h(t), V(t), γ(t), C_L(t) of the GGT are close to the corresponding functions of the OT.

(ii) The characteristic velocity of the GGT is close to the characteristic velocity of the OT. The relative increase in ΔV is 1.3% for Case 1, 0.7% for Case 2, and 0.1% for Case 3.

(iii) The peak heating rate (PHR) of the GGT is somewhat higher than the peak heating rate of the OT. The relative increase in PHR is 9.4% for Case 1, 4.7% for Case 2, and 7.7% for Case 3.

For a particular case (namely, Case 3, GEO-to-LEO transfer), Table 3 compares the results obtained for the OT and the GGT, while Fig. 4 compares the altitude profiles h(t) of the OT and the GGT.

For more detailed information about the behavior of the GGT, see Ref. 17.

5. Modified Gamma Guidance Trajectories

In real AOT flights, there are dispersion effects arising from navigation errors, variations of the atmospheric density, and uncertainties in the aerodynamic coefficients. Navigation errors refer to the space portion of AOT flights and induce errors in the entry path inclination; density variations are due to such factors as latitude, season, time of the day or the night, solar activity or are due to lack of sufficient knowledge of a particular planetary atmosphere (Mars); uncertainties in the aerodynamic coefficients arise because wind tunnel tests

might not simulate precisely the combination of high speeds and low densities characterizing AOT flights or arise because computational fluid dynamics schemes might not account precisely for all of the physical factors involved.

While the gamma guidance scheme of Section 4 yields a trajectory close to the optimal trajectory in the absence of dispersion effects, this scheme is not sufficiently robust with respect to large parameter dispersion. In this connection, there are two ways for improving the stability of the gamma guidance scheme: (i) to decrease the target altitude, while simultaneously increasing the modulus of the entry path inclination; and (ii) to adjust the switch velocity and the target path inclination by means of a predictor-corrector algorithm. The resulting trajectory is called modified gamma guidance trajectory (MGGT).

5.1. Target Altitude and Entry Path Inclination. From the point of view of the total characteristic velocity and the peak heating rate, the target altitude should be as high as possible; hence, it should be as close as possible to the minimum altitude of the optimal trajectory. While the GGT of Section 4 achieves this goal, it is marginally stable with respect to dispersion effects.

With the MGGT, the goal is to increase the stability with respect to dispersion effects, while keeping the total characteristic velocity and the peak heating rate within reasonable range. The increased stability is achieved by lowering the target altitude h_T, hence increasing the target lift coefficient C_{LT}. To achieve compatibility between the target altitude and the entry path inclination γ_0, steeper values of the entry path inclination might be desirable.

5.2. Switch Velocity and Target Path Inclination. Because of parameter dispersion effects, the ideal condition $\Delta V_1 = 0$ cannot be achieved. However, ΔV_1 can be kept small by adjusting the switch velocity and the target path inclination in such a way that ΔV_1 is less than some threshold value specified in advance. This can be achieved via the predictor-corrector algorithm described in Ref. 17 and summarized below.

5.3. Predictor-Corrector Algorithm. The function of the predictor-corrector algorithm is to determine suitable values of V_S, γ_T for given values of γ_0, h_T. Because V_S, γ_T are linearly related to the dimensionless constants A,B via Eqs. (21)-(22), the determination of the pair V_S, γ_T can be replaced with the determination of the pair A,B.

In the predictor-corrector algorithm, it is assumed that the spacecraft is at the end of branch 1, with switch altitude and path inclination given by

$$h_S = h_T, \quad \gamma_S = 0. \tag{24}$$

It is also assumed that the switch velocity is given by Eq. (21) and that the target path inclination is given by Eq.(22).

The algorithm is started with some typical values for the constants A,B (for instance, A = 1/4 and B = 1/2). Then, for branch 2, Eqs. (1)-(3) are integrated in forward time using the feedback control form (17) of the constant path inclination guidance. Once the state of the spacecraft is known at atmospheric exit, one verifies compliance with the inequality

$$\Delta V_1 \leq 0.03 \text{ km/sec.} \qquad (25)$$

If Ineq. (25) is satisfied, the assumed pair (A,B) is accepted. Hence, the assumed pair (V_S, γ_T) is accepted, and the predictor-corrector procedure is terminated.

If Ineq. (25) is violated, one performs two successive one-dimensional searches in the (A,B)-plane. The first search is along the A-direction, while keeping B = const. The second search is along the B-direction, while keeping A = const. The search is terminated whenever a pair A,B is found such that Ineq. (25) is satisfied, subject to suitable safeguards. For more details, see Ref. 17.

5.4. Numerical Results. With reference to Case 3, GEO-to-LEO transfer, we report here on a comparative study of the GGT and the MGGT in the absence of dispersion effects. Dispersion effects are discussed separately in Section 6.

Table 3 compares the results obtained for the GGT and the MGGT, while Table 4 presents typical combinations of the guidance parameters for both the GGT and the MGGT. Figure 4 presents a graphical comparison of the altitude profiles of the GGT and the MGGT.

The main results can be summarized as follows:

(i) The altitude profile of the MGGT lies below the altitude profile of the GGT.

(ii) The velocity and path inclination profiles of the MGGT are relatively close to the corresponding profiles of the GGT.

(iii) The lift coefficient profile of the MGGT is quite different from the lift coefficient profile of the GGT in that an ampler lift coefficient margin now exists with respect to the lower bound value.

(iv) The characteristic velocity of the MGGT is close to the characteristic velocity of the GGT. The relative increase in ΔV is 0.4%.

(v) The peak heating rate of the MGGT is somewhat higher than the peak heating rate of the GGT. The relative increase is 23.9%. The higher peak heating rate of the MGGT is due to deeper penetration into the atmosphere (by 3.1 km), which in turn is tied to the larger value of $|\gamma_0|$ and the lower value of h_T.

For more details on the behavior of the MGGT, see Ref. 17.

6. Dispersion Effects

Here, we report on the behavior of the MGGT vis-a-vis dispersion effects due to navigation errors, variations of the atmospheric density, and uncertainties in the aerodynamic coefficients. We refer to

Case 3, GEO-to-LEO transfer.

For the sake of discussion, let unprimed quantities denote standard values; let primed quantities denote dispersed values; and let the following dispersion factors be defined:

$$F_{\gamma 0} = \gamma_0'/\gamma_0, \tag{26a}$$

$$F_{\rho} = \rho'(h)/\rho(h), \tag{26b}$$

$$F_{CD0} = C_{D0}'/C_{D0}, \tag{26c}$$

$$F_{K} = K'/K, \tag{26d}$$

$$F_{CLR} = (C_{Lb}' - C_{La}')/(C_{Lb} - C_{La}). \tag{26e}$$

Here, $F_{\gamma 0}$ is the entry path inclination factor; F_{ρ} is the density factor; F_{CD0} is the zero-lift drag factor; F_{K} is the induced drag factor; and F_{CLR} is the lift range factor. If there are no dispersion effects,

$$F_{\gamma 0} = 1, \quad F_{\rho} = 1, \tag{27a}$$

$$F_{CD0} = 1, \quad F_{K} = 1, \quad F_{CLR} = 1. \tag{27b}$$

However, if there are dispersion effects, one or more of the above factors might be different from unity.

6.1. Entry Path Inclination Factor. See Table 5 and Fig. 5A. The MGGT is stable for values of the entry path inclination factor in the range

$$0.91 \leq F_{\gamma 0} \leq 1.44, \tag{28a}$$

corresponding to

$$-4.1 \geq \gamma_0 \geq -6.5 \text{ deg}, \tag{28b}$$

$$+0.4 \geq \Delta\gamma_0 \geq -2.0 \text{ deg}. \tag{28c}$$

In the above range, the target altitude, the switch velocity, and the target path inclination are constant. It must be noted that, if $F_{\gamma 0} = 0.89$, corresponding to $\gamma_0 = -4.0$ deg and $\Delta\gamma_0 = +0.5$ deg, the MGGT skips out of the atmosphere. One the other hand, if $F_{\gamma 0} = 1.44$, corresponding to $\gamma_0 = -6.5$ deg and $\Delta\gamma_0 = -2.0$ deg, the MGGT undershoots the target altitude. This situation is due to the fact that only a simple proportional feedback control is used in this paper and can be alleviated by employing more sophisticated forms of feedback control.

6.2. Density Factor. See Table 5 and Fig. 5B. The MGGT is stable for values of the density factor in the range

$$0.33 \leq F_{\rho} < 10.00. \tag{29}$$

In the above range, the entry path inclination, the switch velocity, and the target path inclination are constant. Both the target altitude and the peak heating rate increase as F_{ρ} increases. It is clear from (29) that the modified gamma guidance can tolerate large density increases better than large density decreases. In particular, if $F_{\rho} = 0.25$, the MGGT skips out of the atmosphere with a large increase in characteristic velocity.

6.3. Zero-Lift Drag Factor. See Table 5 and Fig. 5C. The MGGT is stable for values of the zero-lift drag factor in the range

$$0.10 \leq F_{CD0} \leq 5.00. \tag{30}$$

In the above range, the entry path inclination and the target altitude are constant. As F_{CD0} increases, the switch velocity increases, while the flight time decreases considerably. The increase in switch velocity is due to the fact that, as F_{CD0} increases, more energy is depleted for ascending from the target altitude to the atmospheric exit altitude. It is clear from (30) that the modified gamma guidance is able to tolerate both large increases and large decreases in zero-lift drag.

6.4. Induced Drag Factor. See Table 5 and Fig. 5D. The MGGT is stable for values of the induced drag factor in the range

$$0.10 \leq F_K \leq 5.00. \qquad (31)$$

In the above range, the entry path inclination and the target altitude are constant. As F_K increases, the switch velocity increases, while the flight time decreases considerably. The increase in switch velocity is due to the fact that, as F_K increases, more energy is depleted for ascending from the target altitude to the atmospheric exit altitude. It is clear from (31) that the modified gamma guidance is able to tolerate both large increases and large decreases in induced drag.

6.5. Lift Range Factor. See Table 5 and Fig. 5E. The MGGT is stable for values of the lift range factor such that

$$0.33 \leq F_{CLR} \leq 3.00. \qquad (32)$$

In the above range, the entry path inclination and the target path inclination are constant. As F_{CLR} increases, the target altitude increases, the switch velocity decreases, and the target lift coefficent, which is negative, becomes larger in modulus; indeed, C_{LT} is proportional to F_{CLR}. As F_{CLR} increases, the peak heating rate decreases considerably, and the flight time changes somewhat. Generally speaking, the MGGT is more able to tolerate large increases in F_{CLR} than large decreases. In particular, if $F_{CLR} = 0.25$, the MGGT skips out of the atmosphere with a large increase in characteristic velocity.

7. Conclusions

With reference to the optimization and guidance of trajectories for coplanar, aeroassisted orbital transfer, the following major conclusions are obtained:

(i) The optimal trajectories include two branches: a relatively short descending flight branch (branch 1) and a long ascending flight branch (branch 2). In branch 1, the path inclination is nearly a linear function of the altitude; in branch 2, the path inclination is a slowly varying function of the altitude.

(ii) Gamma guidance trajectories are developed. They employ a feedback control scheme in which the lift coefficient is adjusted according to a two-stage gamma guidance law. For branch 1, the gamma guidance is a linear path inclination guidance; for branch 2, the gamma guidance is a constant path inclination guidance. By properly selecting four guidance parameters (the entry path inclination, the target altitude, the switch velocity, and

the target path inclination), the gamma guidance trajectory can be made close to the optimal trajectory.

(iii) Improvements in stability are possible via a modified gamma guidance, which differs from the gamma guidance in two aspects: lower target altitude, coupled with steeper entry path inclination; and use of a predictor-corrector algorithm to adjust the values of the switch velocity and the target path inclination. Computer simulations show that the modified gamma guidance trajectory is quite stable with respect to dispersion effects arising from navigation errors, variations of the atmospheric density, and uncertainties in the aerodynamic coefficients.

(iv) A byproduct of the dispersion studies is the following design concept. For coplanar, aeroassisted orbital transfer, the lift-range-to-weight ratio appears to play a more important role than the lift-to-drag ratio. This is because the lift-range-to-weight ratio controls mainly the minimum altitude (hence, the peak heating rate) of the guidance trajectory; on the other hand, the lift-to-drag ratio controls mainly the duration of the atmospheric pass of the guidance trajectory.

References

1. MEASE, K. D., and VINH, N. X., "Minimum-Fuel Aeroassisted Coplanar Orbit Transfer Using Lift Modulation", Journal of Guidance, Control, and Dynamics, Vol. 8, No. 1, pp. 134-141, January-February 1985.
2. MIELE, A., BASAPUR, V. K., and MEASE, K. D., "Nearly-Grazing Optimal Trajectories for Aeroassisted Orbital Transfer", Journal of the Astronautical Sciences, Vol. 34, No. 1, pp. 3-18, January-March 1986.
3. MIELE, A., BASAPUR, V. K., and LEE, W. Y., "Optimal Trajectories for Aeroassisted, Coplanar Orbital Transfer", Journal of Optimization Theory and Applications, Vol. 52, No. 1, pp. 1-24, January 1987.
4. MEASE, K. D., "Optimization of Aeroassisted Orbital Transfer: Current Status", Journal of the Astronautical Sciences, Vol. 36, Nos. 1-2, pp. 7-33, January-June 1988.
5. MIELE, A., WANG, T., LEE, W. Y., and ZHAO, Z. G., "Optimal Trajectories for the Aeroassisted Flight Experiment", Paper No. IAF-89-361, 40th Congress of the International Astronautical Federation, Malaga, Spain, 1989.
6. VINH, N. X., JOHANNESEN, J. R., MEASE, K. D., and HANSON, J. M., "Explicit Guidance of Drag-Modulated Aeroassisted Transfer between Elliptical Orbits", Journal of Guidance, Control, and Dynamics, Vol. 9, No. 3, pp. 274-280, May-June 1986.
7. MEASE, K. D., and McCREARY, F. A., "Atmospheric Guidance Law for Planar Skip Trajectories", Paper No.

AIAA-85-1818, AIAA 12th Atmospheric Flight Mechanics Conference, Snowmass, Colorado, 1985.

8. LEE, B. S., and GRANTHAM, W. J., "Aeroassisted Orbital Maneuvering Using Lyapunov Optimal Feedback Control", Journal of Guidance, Control, and Dynamics, Vol. 12, No. 2, pp. 237-242, March-April 1989.

9. GAMBLE, J. D., CERIMELE, C. J., MOORE, T. E., and HIGGINS, J., "Atmospheric Guidance Concepts for an Aeroassist Flight Experiment", Journal of the Astronautical Sciences, Vol. 36, Nos. 1-2, pp. 45-71, January-June 1988.

10. MIELE, A., WANG, T., and LEE, W. Y., "Optimization and Guidance of Trajectories for Coplanar, Aeroassisted Orbital Transfer", Aero-Astronautics Report No. 241, Rice University, 1989.

11. MIELE, A., WANG, T., TZENG, C. Y., and MELVIN, W. W., "Abort Landing Guidance Trajectories in the Presence of Windshear", Journal of the Franklin Institute, Vol. 326, No. 2, pp. 185-220, February 1989.

12. MIELE, A., WANG, T., MELVIN, W. W., and BOWLES, R. L., "Acceleration, Gamma, and Theta Guidance for Abort Landing in a Windshear", Journal of Guidance, Control, and Dynamics, Vol. 12, No. 6, pp. 815-821, November-December 1989.

13. NOAA, NASA, and USAF, "US Standard Atmosphere, 1976", US Government Printing Office, Washington, DC, 1976.

14. MIELE, A., WANG, T., and BASAPUR, V. K., "Primal and Dual Formulations of Sequential Gradient-Restoration Algorithms for Trajectory Optimization Problems", Acta Astronautica, Vol. 13, No. 8, pp. 491-505, August 1986.

15. MIELE, A., and WANG, T., "Primal-Dual Properties of Sequential Gradient-Restoration Algorithms for Optimal Control Problems, Part 1, Basic Problem", Integral Methods in Science and Engineering, Edited by F. R. Payne et al, Hemisphere Publishing Corporation, Washington, DC, pp. 577-607, 1986.

16. MIELE, A., and WANG, T., "Primal-Dual Properties of Sequential Gradient-Restoration Algorithms for Optimal Control Problems, Part 2, General Problem", Journal of Mathematical Analysis and Applications, Vol. 119, Nos. 1-2, pp. 21-54, October-November 1986.

17. MIELE, A., and WANG, T., "Gamma Guidance of Trajectories for Coplanar, Aeroassisted Orbital Transfer", Aero-Astronautics Report No. 246, Rice University, 1990.

Table 1. OT results.

Quantity	Case 1	Case 2	Case 3	Units
h_0	120.0	120.0	120.0	km
V_0	9.040	9.905	10.310	km/sec
γ_0	-3.034	-3.893	-4.204	deg
h_1	120.0	120.0	120.0	km
V_1	7.844	7.844	7.844	km/sec
γ_1	0.319	0.319	0.319	deg
h_{min}	79.50	76.35	75.36	km
PHR	35.90	59.61	72.70	W/cm^2
τ	2.147	2.297	2.347	ksec
ΔV_{00}	1.025	1.445	1.490	km/sec
ΔV_1	0.000	0.000	0.000	km/sec
ΔV_{11}	0.025	0.025	0.025	km/sec
ΔV	1.049	1.470	1.515	km/sec

Table 2. GGT parameters.

Quantity	Case 1	Case 2	Case 3	Units
γ_0	-3.300	-4.100	-4.400	deg
h_T	78.25	75.75	74.32	km
V_S	8.700	9.180	9.400	km/sec
γ_T	0.115	0.113	0.114	deg

Table 3. OT, GGT, and MGGT results, Case 3 (no dispersion).

Quantity	OT	GGT	MGGT	Units
h_0	120.0	120.0	120.0	km
V_0	10.310	10.310	10.310	km/sec
γ_0	-4.204	-4.400	-4.500	deg
h_1	120.0	120.0	120.0	km
V_1	7.844	7.841	7.835	km/sec
γ_1	0.319	0.300	0.245	deg
h_{min}	75.36	74.28	71.14	km
PHR	72.70	78.27	96.97	W/cm^2
τ	2.347	2.405	3.012	ksec
ΔV_{00}	1.490	1.490	1.491	km/sec
ΔV_1	0.000	0.003	0.011	km/sec
ΔV_{11}	0.025	0.024	0.022	km/sec
ΔV	1.515	1.517	1.523	km/sec

Table 4. GGT and MGGT parameters, Case 3 (no dispersion).

Quantity	GGT	MGGT	Units
γ_0	-4.400	-4.500	deg
h_T	74.32	71.14	km
V_S	9.400	8.400	km/sec
γ_T	0.114	0.150	deg

Table 5. Dispersion effects, MGGT, Case 3.

Dispersion factor	γ_0 deg	h_T km	V_S km/sec	γ_T deg	PHR W/cm^2	τ ksec	ΔV km/sec
$F_{\gamma 0}$ = 0.91	-4.1	71.14	8.40	0.15	83.79	2.986	1.523
$F_{\gamma 0}$ = 1.00	-4.5	71.14	8.40	0.15	96.97	3.012	1.523
$F_{\gamma 0}$ = 1.44	-6.5	71.14	8.40	0.15	180.80	2.810	1.529
F_{ρ} = 0.33	-4.5	62.98	8.40	0.15	87.66	3.670	1.535
F_{ρ} = 1.00	-4.5	71.14	8.40	0.15	96.97	3.012	1.523
F_{ρ} = 10.00	-4.5	85.84	8.40	0.15	127.67	2.376	1.519
F_{CD0}= 0.10	-4.5	71.14	8.20	0.15	98.96	4.268	1.547
F_{CD0}= 1.00	-4.5	71.14	8.40	0.15	96.97	3.012	1.523
F_{CD0}= 5.00	-4.5	71.14	9.10	0.21	90.00	1.953	1.534
F_K = 0.10	-4.5	71.14	8.15	0.15	103.63	4.281	1.523
F_K = 1.00	-4.5	71.14	8.40	0.15	96.97	3.012	1.523
F_K = 5.00	-4.5	71.14	9.10	0.25	83.95	1.646	1.541
F_{CLR}= 0.33	-4.5	62.98	9.00	0.15	174.29	2.390	1.555
F_{CLR}= 1.00	-4.5	71.14	8.40	0.15	96.97	3.012	1.523
F_{CLR}= 3.00	-4.5	78.41	8.40	0.15	49.08	2.571	1.533

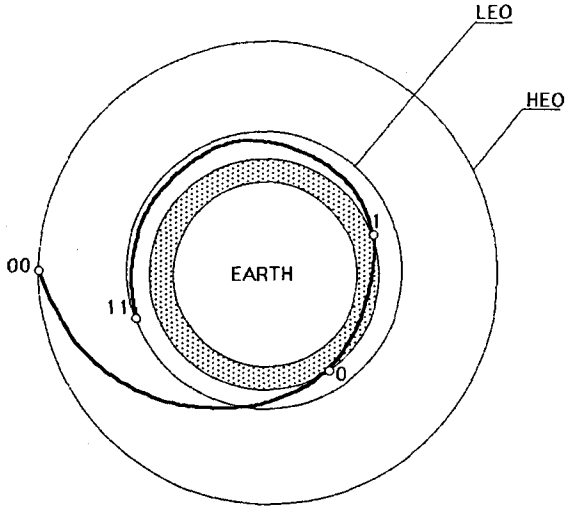

Fig.1. Coplanar, aeroassisted orbit transfer.

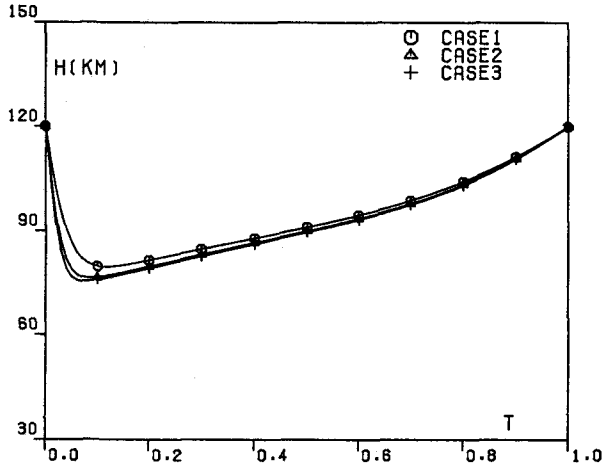

FIG. 2A. OPTIMAL TRAJECTORIES.

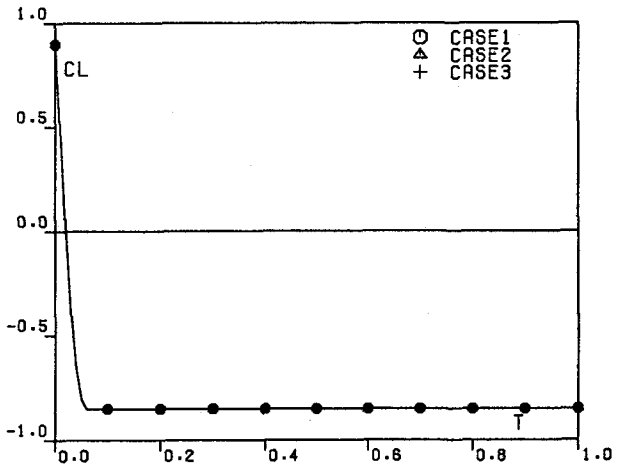

FIG. 2D. OPTIMAL TRAJECTORIES.

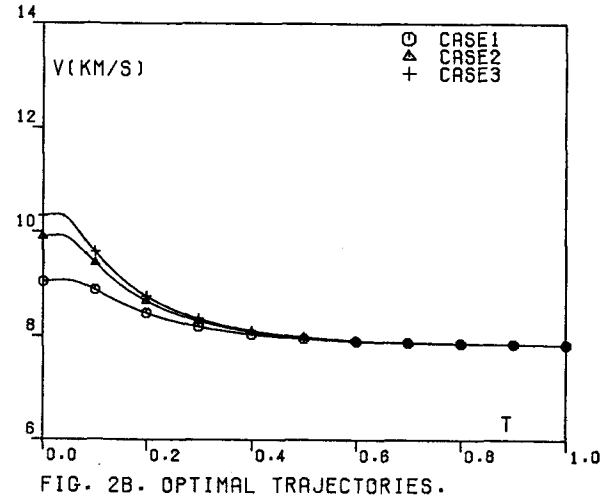

FIG. 2B. OPTIMAL TRAJECTORIES.

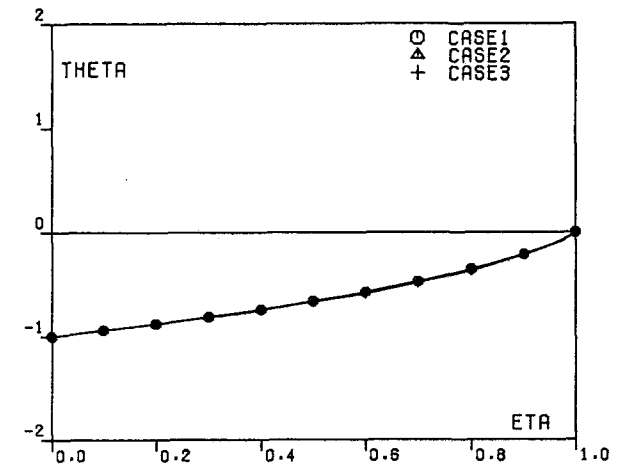

FIG. 3A. OPTIMAL TRAJECTORIES.
BRANCH 1.

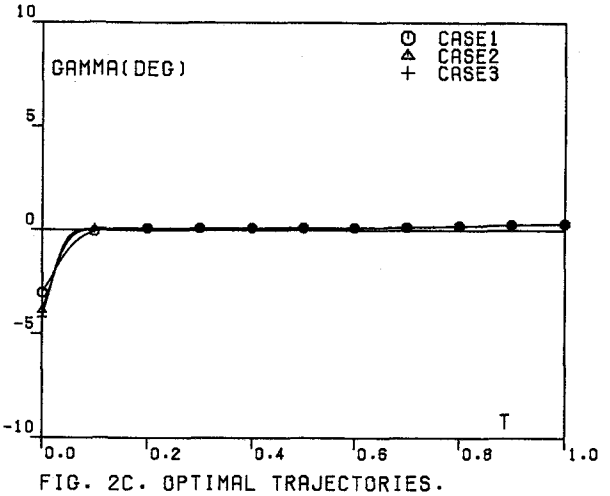

FIG. 2C. OPTIMAL TRAJECTORIES.

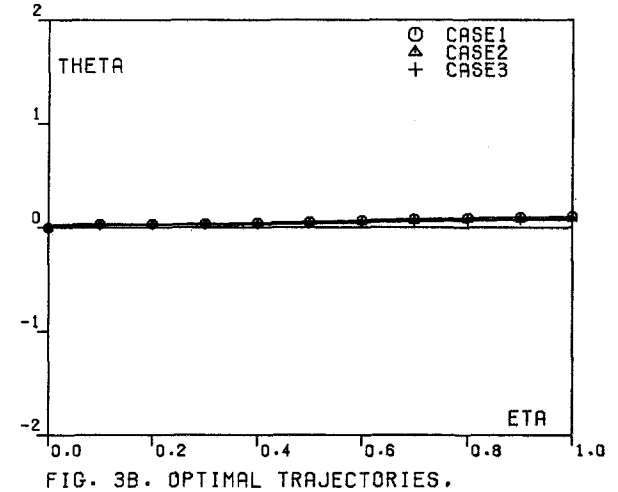

FIG. 3B. OPTIMAL TRAJECTORIES.
BRANCH 2.

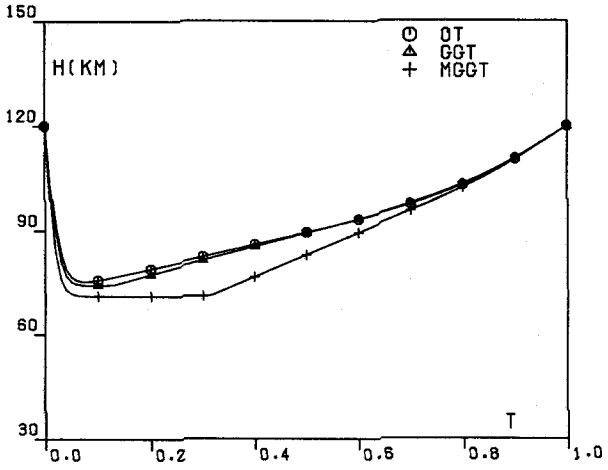

FIG. 4. TRAJECTORY COMPARISON, CASE3.

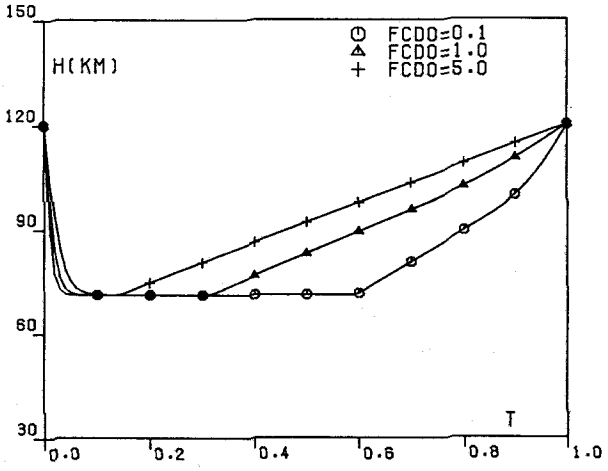

FIG. 5C. MODIFIED GUIDANCE TRAJECTORIES, ZERO-LIFT DRAG CHANGE, CASE3.

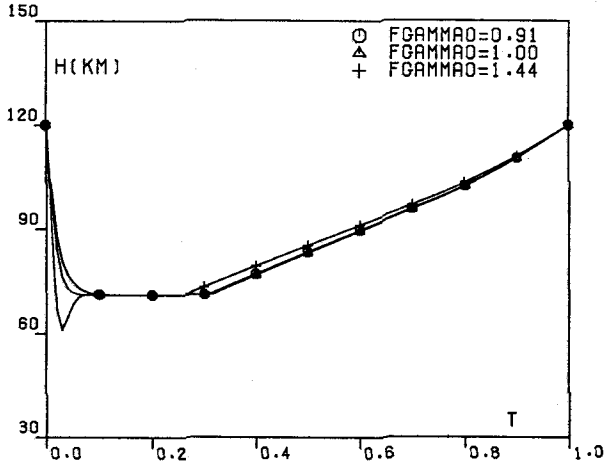

FIG. 5A. MODIFIED GUIDANCE TRAJECTORIES, ENTRY GAMMA CHANGE, CASE3.

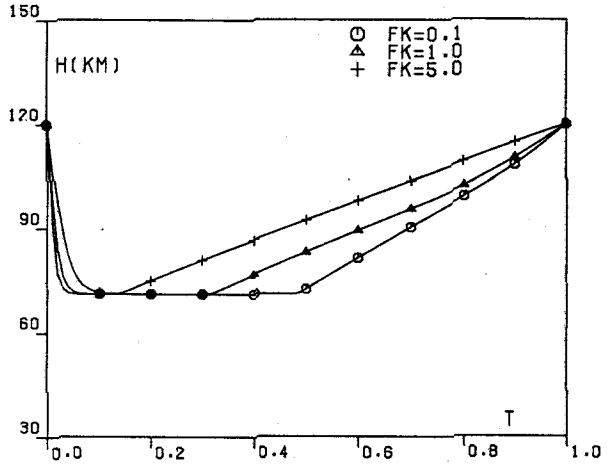

FIG. 5D. MODIFIED GUIDANCE TRAJECTORIES, INDUCED DRAG CHANGE, CASE3.

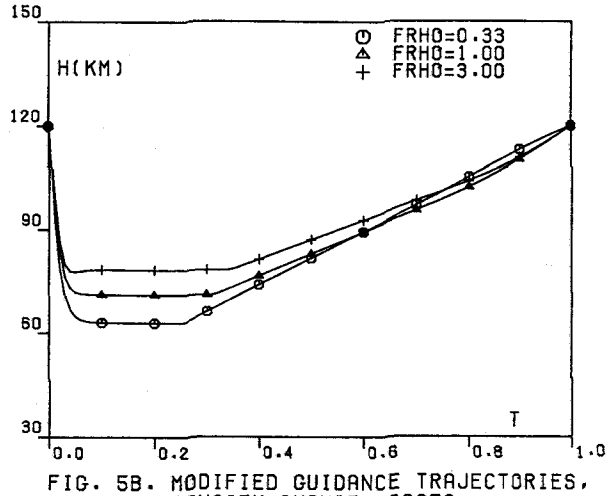

FIG. 5B. MODIFIED GUIDANCE TRAJECTORIES, DENSITY CHANGE, CASE3.

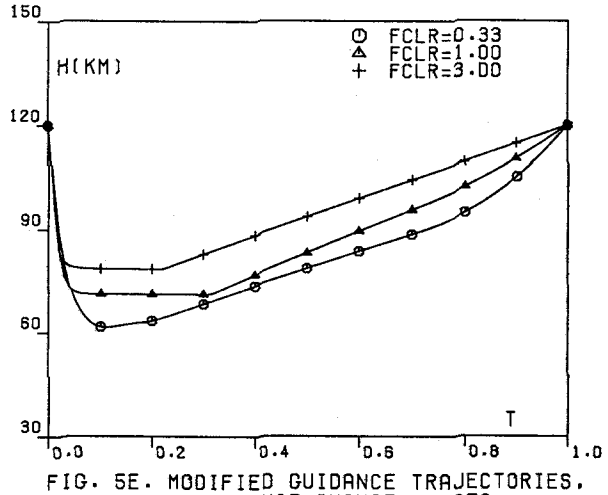

FIG. 5E. MODIFIED GUIDANCE TRAJECTORIES, LIFT RANGE CHANGE, CASE3.